Supporting Information

Spectral and Spatial Characterization of Upconversion Luminescence Nanocrystals as Nanowaveguides

Wen Xu[1,2], *Tae Kyung Lee*[3], *Byeong-Seok Moon*[4,5], *Donglei Zhou*[2], *Hongwei Song*[2], *Young-Jin Kim*[6], *Sang Kyu Kwak**[3], *Peng Chen**[1], *Dong-Hwan Kim**[4]

[1]School of Chemical and Biomedical Engineering, Nanyang Technological University, 50 Nanyang Avenue, Singapore 639798, Singapore

[2]State Key Laboratory on Integrated Optoelectronics, College of Electronic Science and Engineering, Jilin University, 2699 Qianjin Street, Changchun 130012, China

[3]School of Energy and Chemical Engineering, Ulsan National Institute of Science and Technology (UNIST), Ulsan 44919, South Korea

[4]School of Chemical Engineering, Sungkyunkwan University 16419, Republic of Korea

[5]Department of Materials Science and Engineering, Seoul National University, Seoul 151-742, Republic of Korea

[6]School of Mechanical and Aerospace Engineering, Nanyang Technological University, 50 Nanyang Avenue, Singapore 639798, Singapore

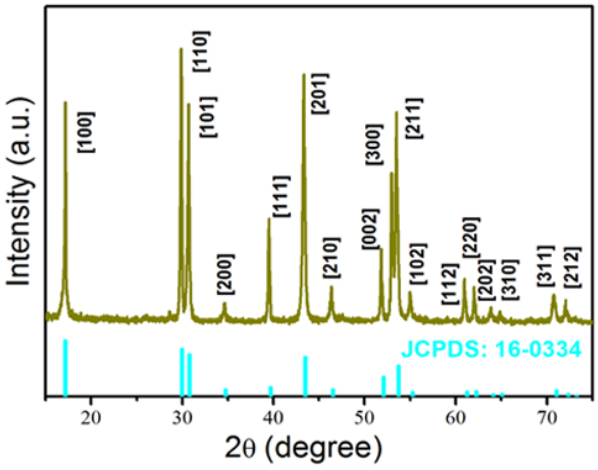

Figure S1 XRD pattern of $NaYF_4$:RE nanowire powder and the standard card of β-$NaYF_4$.

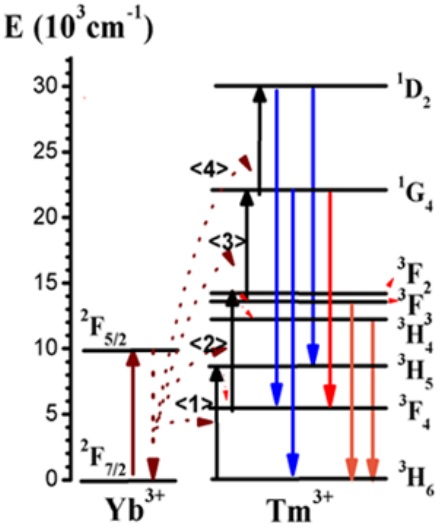

Figure S2 Upconversion emission process of Yb^{3+},Tm^{3+} co-doped $NaYF_4$.

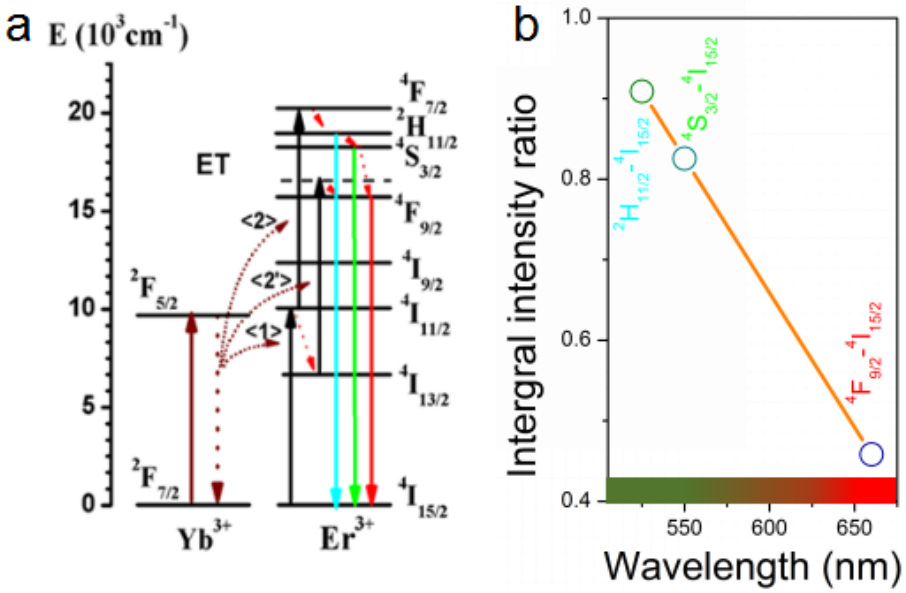

Figure S3 (a) Schematic of the UC populating mechanism for $NaYF_4$:Yb^{3+},Er^{3+}. (b) Integral UCL intensity ratio between the end and the middle points at different emission wavelengths in a single $NaYF_4$:Yb^{3+},Er^{3+} nanowire under 980-nm excitation. The multiband emissions of Yb^{3+},Er^{3+} ion-doped $NaYF_4$ are assigned to $^2H_{11/2}\rightarrow{}^4I_{15/2}$ at 525 nm, $^4S_{3/2}\rightarrow{}^4I_{15/2}$ at 550 nm, and $^4F_{9/2}\rightarrow{}^4I_{15/2}$ at 660 nm. The corresponding UC populating mechanism is shown in Fig. S3(a). Interestingly, compared with the end and middle emissions of a single $NaYF_4$:Yb^{3+},Er^{3+} nanowire, the long-wavelength emissions in the middle of the nanowire are enhanced in a wavelength-dependent manner.

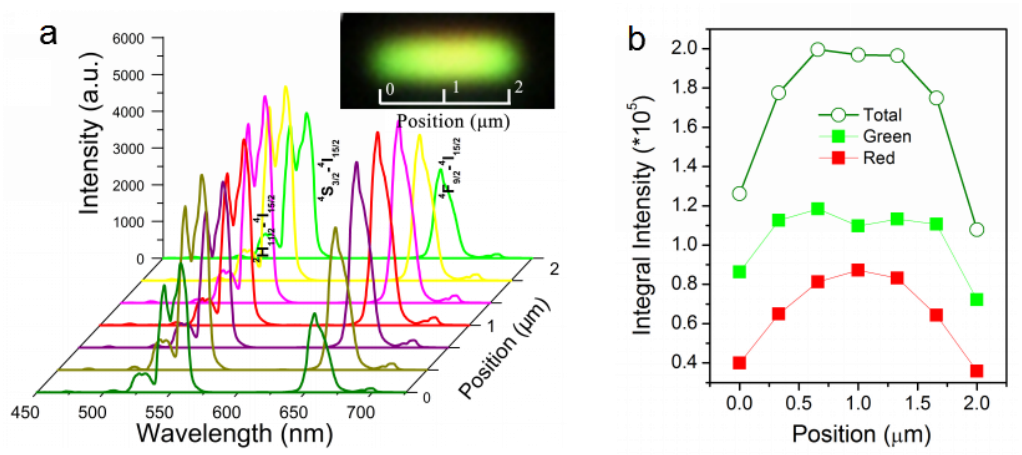

Figure S4 (a) Upconversion luminescence spectra at different points in a single $NaYF_4$:Yb^{3+},Er^{3+} nanowire under 980-nm illumination. (b) Integral intensity of green emissions ($^2H_{11/2}$,$^4S_{3/2}$-$^4I_{15/2}$), red emissions ($^4F_{9/2}$-$^4I_{15/2}$), and total emissions at different positions in the $NaYF_4$:Yb^{3+},Er^{3+} nanowire.

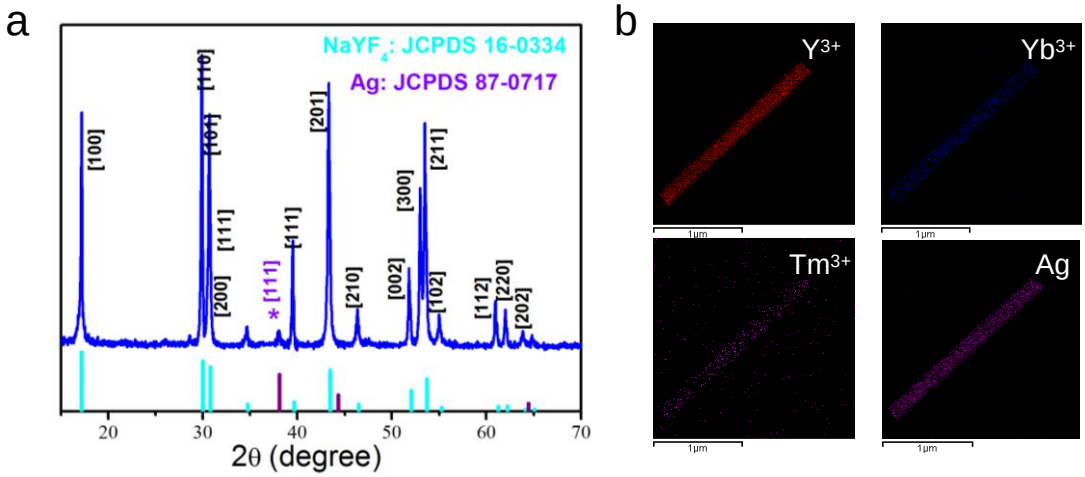

Figure S5 (a) XRD pattern of $NaYF_4$:Yb^{3+},Tm^{3+}@Ag nanowires and the standard cards of β-$NaYF_4$ and cubic Ag. The peak marked with an asterisk (*) originates from the diffusion peak of the [111] face of cubic Ag, which confirms the formation of the $NaYF_4$:Yb^{3+},Tm^{3+}@Ag nanowire. (b) Elemental mapping of a single $NaYF_4$:Yb^{3+},Tm^{3+}@Ag nanowire.

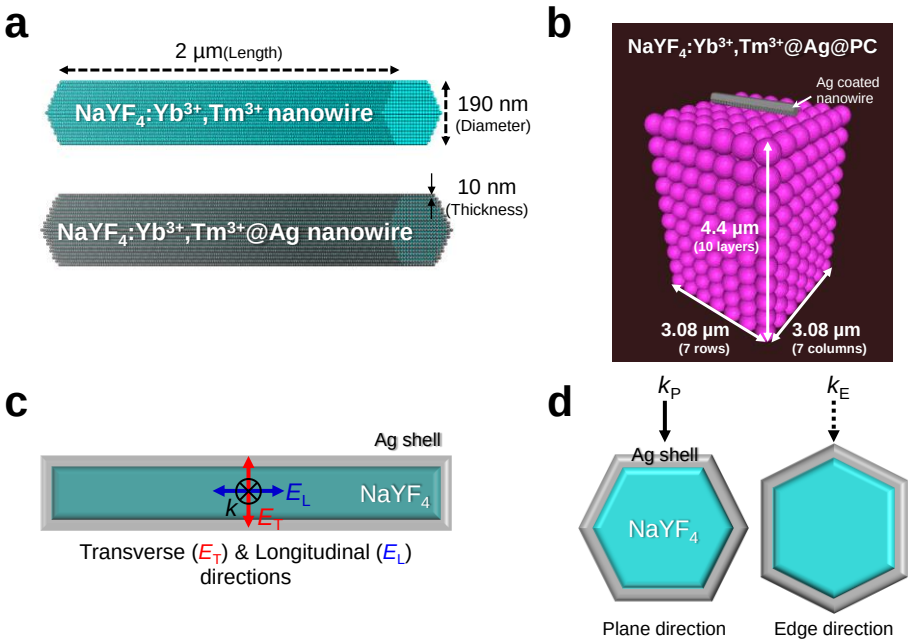

Figure S6 Model systems for discrete dipole approximation (DDA) calculation. (a) Model systems of $NaYF_4:Yb^{3+},Tm^{3+}$ (190 nm in diameter and 2 μm in length) and $NaYF_4:Yb^{3+},Tm^{3+}$@Ag ($NaYF_4:Yb^{3+},Tm^{3+}$ nanowire with 10-nm Ag shell) nanowires. These model systems have 59,800 and 72,518 dipoles, respectively. (b) Model system of an $NaYF_4:Yb^{3+},Tm^{3+}$@Ag@PC nanowire ($NaYF_4:Yb^{3+},Tm^{3+}$@Ag nanowire on a PMMA photonic crystal of 7 rows (3.08 μm) × 7 columns (3.08 μm) × 10 layers (4.4 μm)) with 21,985,318 dipoles. The image in (b) was obtained using LiteBil ver. 0.9.5b. (c) The incident electric field is applied in two directions: transverse (E_T, red arrow) and longitudinal (E_L, blue arrow). The transverse (longitudinal) direction means that the direction of the electric field is perpendicular (parallel) to the principal axis of the nanowire. *k* (black arrow) represents the direction of the incident light. (d) Cross-section of the hexagonal nanowire structure. Light is applied in two directions: the plane (k_P, solid black arrow) and edge (k_E, dotted black arrow) directions. When the light is propagated to the plane (edge) region of a hexagonal nanowire, we define it as being in the plane (edge) direction.

Supplementary Note 1. Model systems for DDA calculation. According to the size information of the synthesized $NaYF_4:Yb^{3+},Tm^{3+}$; $NaYF_4:Yb^{3+},Tm^{3+}$@Ag; and $NaYF_4:Yb^{3+},Tm^{3+}$@Ag@ PC nanowire systems used in the experiment, we constructed model systems for the DDA calculation (Fig. S6(a) and S6(b)). The $NaYF_4:Yb^{3+},Tm^{3+}$ nanowire model shown in Fig. S6(a) has a diameter of 190 nm and a length of 2 μm. The cross-sectional shape of the nanowire was assumed to be hexagonal. For a $NaYF_4:Yb^{3+},Tm^{3+}$@Ag nanowire, the model system was considered to be a $NaYF_4:Yb^{3+},Tm^{3+}$ nanowire with a 10-nm Ag coating. In Fig. S6(b), the $NaYF_4:Yb^{3+},Tm^{3+}$@Ag@PC nanowire is modeled as a $NaYF_4:Yb^{3+},Tm^{3+}$@Ag nanowire in the center of a 7 row (3.08 μm) × 7 column (3.08 μm) × 10 layer (4.4 μm) PMMA photonic crystal. The diameter of one PMMA bead was 440 nm. The numbers of dipoles were 59,800, 72,518, and 21,985,318 for the $NaYF_4:Yb^{3+},Tm^{3+}$; $NaYF_4:Yb^{3+},Tm^{3+}$@Ag; and $NaYF_4:Yb^{3+},Tm^{3+}$@Ag@PC nanowires, respectively.

Then, as shown in Fig. S6(c) and S6(d), we considered the two cases of the directions of the incident electric field and light. First, the transverse (E_T) and longitudinal (E_L) directions were considered for the electric field (Fig. S6(c)). When the direction of the electric field is perpendicular to the principal axis of the nanowire, it is defined as the transverse direction, and the generated mode is defined as the transverse mode. On the other hand, the longitudinal direction and mode are generated if the electric field is parallel to the principal axis. Second, there are the two directions in which the incident light (k) propagates onto the hexagonal nanowire structure. These cases are denoted as the "plane direction" (k_P) and "edge direction" (k_E) (Fig. S6(d)).

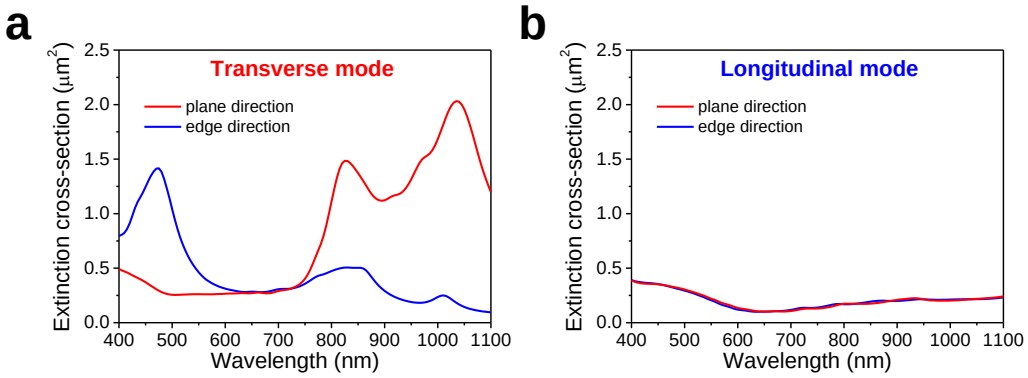

Figure S7 Simulated extinction spectra of an $NaYF_4$:Yb^{3+},Tm^{3+}@Ag nanowire in the (a) transverse and (b) longitudinal modes. In each mode, the plane (red line) and edge (blue line) directions of incident light are considered.

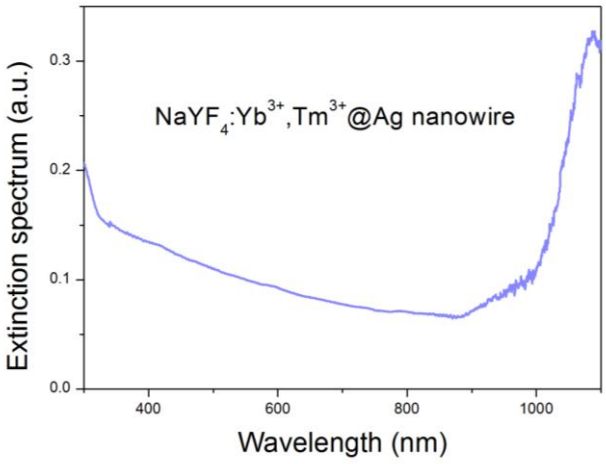

Figure S8 Extinction spectrum of an $NaYF_4$:Yb^{3+},Tm^{3+}@Ag nanowire.

Supplementary Note 2. Extinction spectra of $NaYF_4$:Yb^{3+},Tm^{3+}@Ag nanowire according to two types of directional-dependence factors. Considering the two types of directional-dependence factors (i.e., the directions of the incident electric field and light; Supplementary Note 1), we calculated the extinction spectra of the $NaYF_4$:Yb^{3+},Tm^{3+}@Ag nanowire to investigate the characteristic of the plasmonic effect of the Ag coating. In Fig. S7(a), in the transverse (E_T) mode, the extinction spectra exhibit high intensities with peaks comparable to those in the longitudinal mode (Fig. S7(b)). In particular, the plane (k_P) direction of the light causes the extinction spectra to increase rapidly with the wavelength, while two peaks are generated at wavelengths of approximately 825 and 1,035 nm. The experimental extinction spectrum (Fig. S8) exhibits a similar trend to the simulated spectrum for the E_T mode in an $NaYF_4$:Yb^{3+},Tm^{3+}@Ag nanowire. Given this result, we predict that an $NaYF_4$:Yb^{3+},Tm^{3+}@Ag nanowire exposed to light traveling in the k_P direction in the E_T mode exhibits a high absorption of photons at a wavelength of 980 nm.

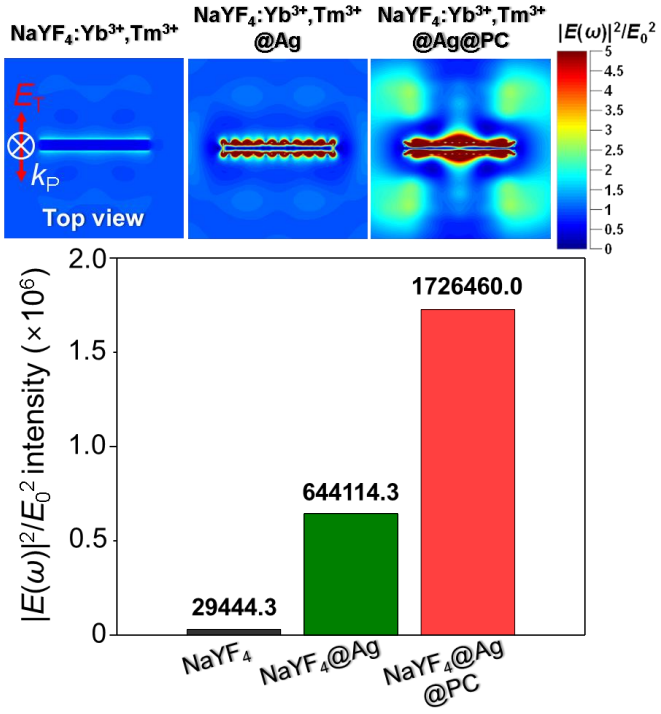

Figure S9 Top views of the $|E(\omega)|^2/E_0^2$ distributions of $NaYF_4$:Yb^{3+},Tm^{3+}; $NaYF_4$:Yb^{3+},Tm^{3+}@Ag; and $NaYF_4$:Yb^{3+},Tm^{3+}@Ag@PC nanowire systems and the total $|E(\omega)|^2/E_0^2$ intensities of $NaYF_4$:Yb^{3+},Tm^{3+} in each system under plane-direction incident light (k_p, white arrow) and the transverse (E_T, red solid arrow) mode of the incident electric field at a wavelength of 980 nm.

Supplementary Note 3. Electric-field distribution of $NaYF_4$:Yb^{3+},Tm^{3+}@Ag and $NaYF_4$:Yb^{3+},Tm^{3+}@Ag@PC nanowires. We calculated the $|E(\omega)|^2/E_0^2$ intensity using a DDA calculation in which two types of directional dependences of the incident electric field (i.e., the longitudinal (E_L) and transverse (E_T) directions) and incident light (i.e., plane (k_P) and edge (k_E) directions) were considered. According to the simulated and experimental extinction spectra (Figs. S7, S8, and Supplementary Note 2), we calculated the total $|E(\omega)|^2/E_0^2$ intensity of $NaYF_4$:Yb^{3+},Tm^{3+} for each nanowire model system in the k_P direction and the E_T mode at a wavelength of 980 nm (Figs. S9). We conjecture that the main factor leading to the difference is most likely the k_P direction in the E_T mode where the effect of the plasmon is maximized at 980 nm wavelength.

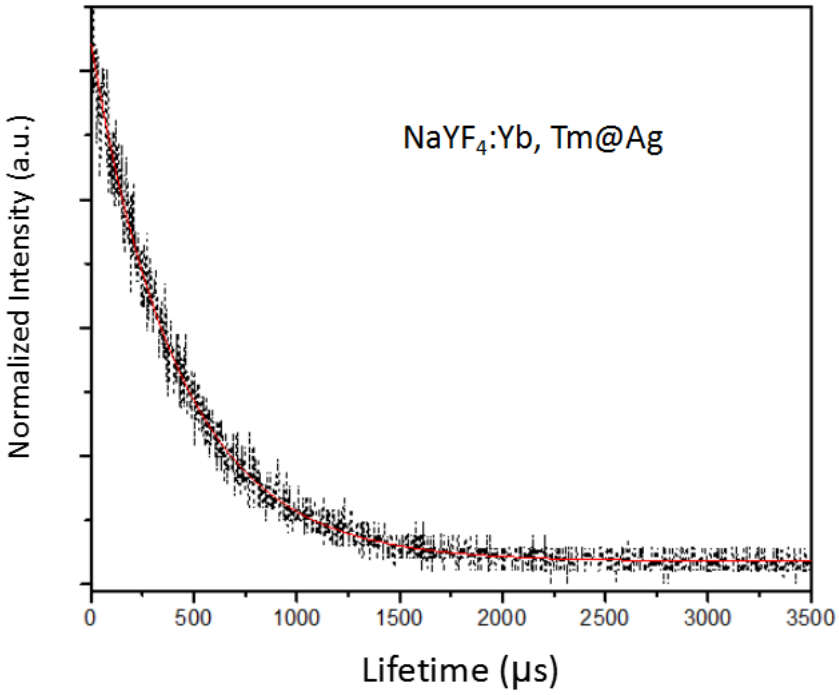

Figure S10 Lifetime (blue emissions) of monodispersed $NaYF_4$:Yb^{3+},Tm^{3+}@Ag nanocrystals. Via single exponential fitting, its lifetime is determined to be 430 μs.

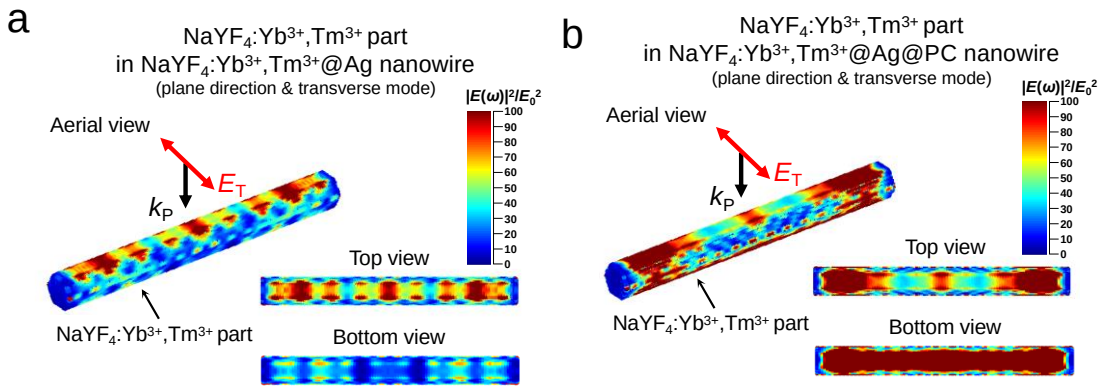

Figure S11 (a, b) Three views (aerial, top, and bottom views) of the $|E(\omega)|^2/E_0^2$ distributions for the $NaYF_4$:Yb^{3+},Tm^3 of (a) $NaYF_4$:Yb^{3+},Tm^{3+}@Ag and (b) $NaYF_4$:Yb^{3+},Tm^{3+}@ Ag@PC nanowires with plane (k_P, black arrow)-direction incident light in the transverse (E_T, red arrow) mode of the electric field at a wavelength of 980 nm.

Supplementary Note 4. Electric-field distribution of $NaYF_4$:Yb^{3+},Tm^{3+}@Ag and $NaYF_4$:Yb^{3+},Tm^{3+}@Ag@PC nanowires. We investigated the electric-field distributions according to the intensity profiles of $|E(\omega)|^2/E_0^2$ of the $NaYF_4$:Yb^{3+},Tm^{3+} in $NaYF_4$:Yb^{3+},Tm^{3+}@Ag and $NaYF_4$:Yb^{3+},Tm^{3+}@Ag@PC nanowire systems under the k_P direction and the E_T mode at a wavelength of 980 nm (Fig. S11). When partial enhancements, which are distributed over the sites for both nanowire systems (Fig. S11), are integrated, the $|E(\omega)|^2/E_0^2$ intensity profile reveals a greater enhancement at the ends than in the middle for both systems. This leads to larger UCL enhancements at the ends than in the middle for both the $NaYF_4$:Yb^{3+},Tm^{3+}@Ag and $NaYF_4$:Yb^{3+},Tm^{3+}@Ag@PC nanowires. In addition, the end positions have higher electric-field intensities than the middle positions at wavelengths around 450 nm (Fig. 4(j)).